

Geophysical Research Letters®



RESEARCH LETTER

10.1029/2024GL109000

Key Points:

- Predominantly red-line auroras are linked to flow bursts, TDSs, and <1 keV electron precipitation
- For the first time, red-line diffuse-like auroras have been forward-modeled using TReX-ATM with time domain structure (TDS) inputs
- A good correlation between forward-modeled and observed red-line emissions suggests that TDSs are a major driver

Supporting Information:

Supporting Information may be found in the online version of this article.

Correspondence to:










Y. Shen,
yshen@epss.ucla.edu

Citation:

Shen, Y., Liang, J., Artemyev, A., Angelopoulos, V., Ma, Q., Lyons, L., et al. (2024). Red line diffuse-like aurora driven by time domain structures associated with braking magnetotail flow bursts. *Geophysical Research Letters*, *51*, e2024GL109000. <https://doi.org/10.1029/2024GL109000>

Received 27 FEB 2024
Accepted 15 APR 2024

Red Line Diffuse-Like Aurora Driven by Time Domain Structures Associated With Braking Magnetotail Flow Bursts

Yangyang Shen¹ , Jun Liang² , Anton Artemyev^{1,3} , Vassilis Angelopoulos¹ , Qianli Ma^{4,5}, Larry Lyons⁴ , Jiang Liu¹ , Yukitoshi Nishimura⁵ , Xiao-Jia Zhang⁶ , Ivan Vasko⁶, and Donald L. Hampton⁷ 

¹Department of Earth, Planetary, and Space Sciences, University of California, Los Angeles, Los Angeles, CA, USA, ²Department of Physics and Astronomy, University of Calgary, Calgary, AB, Canada, ³Space Research Institute of Russian Academy of Sciences, RussiaMoscow, ⁴Department of Atmospheric and Oceanic Sciences, University of California, Los Angeles, Los Angeles, CA, USA, ⁵Center for Space Physics, Boston University, Boston, MA, USA, ⁶William B. Hanson Center for Space Sciences, University of Texas at Dallas, Richardson, TX, USA, ⁷Geophysical Institute, University of Alaska Fairbanks at Fairbanks, Fairbanks, AK, USA

Abstract Magnetotail earthward-propagating fast plasma flows provide important pathways for magnetosphere-ionosphere coupling. This study reexamines a flow-related red-line diffuse-like aurora event previously reported by Liang et al. (2011, <https://doi.org/10.1029/2010ja015867>), utilizing THEMIS and ground-based auroral observations from Poker Flat. We find that time domain structures (TDSs) within the flow bursts efficiently drive electron precipitation below a few keV, aligning with predominantly red-line auroral intensifications in this non-substorm event. The diffuse-like auroras sometimes coexisted with or potentially evolved from discrete forms. We forward model red-line diffuse auroras due to TDS-driven precipitation, employing the time-dependent TReX-ATM auroral transport code. The good correlation (~0.77) between our modeled and observed red line emissions underscores that TDSs are a primary driver of the red-line diffuse-like auroras, though whistler-mode wave contributions are needed to fully explain the most intense red-line emissions.

Plain Language Summary Fast plasma flows in the magnetotail, traveling earthward at several hundred kilometers per second, transport energetic particles and magnetic flux into the inner magnetosphere. Upon braking near Earth's high magnetic flux regions, they trigger plasma instabilities and waves, leading to increased electric currents and particle precipitation in the polar regions. This precipitation, depending on its driver, results in either diffuse auroras from electron pitch-angle scattering, or discrete auroras from field-aligned electron acceleration and currents. Our case study highlights the important role of time-domain structures in diffuse-like aurora generation during flow braking. This reveals a new aspect of magnetosphere-ionosphere coupling: the generation of diffuse auroras through electron scattering by time-domain structures in braking flow bursts.

1. Introduction

Since their discovery in the 1970's (Gurnett et al., 1976; Scarf et al., 1974), broadband electrostatic noise in the frequency range of tens of Hz up to several kHz have been observed to be ubiquitous in various space plasmas (Cattell et al., 2005; Ergun et al., 1998; Williams et al., 2006). These fluctuations, when examined in the time domain (Matsumoto et al., 1994), manifest unique localized electrostatic solitary structures, comprising mostly electron phase-space holes and double layers, which are collectively termed as time-domain structures (TDSs) (Mozer et al., 2015).

Recently, there have been active discussions on the role of TDS-induced electron scattering in generating diffuse auroras (Mozer et al., 2018; Nishimura et al., 2018; Shen et al., 2020, 2021; Vasko et al., 2017, 2018). While Mozer et al. (2018) proposed that TDSs contribute to electron precipitation into pulsating auroras, Nishimura et al. (2018) argued that TDSs were more likely linked to discrete auroras or non-pulsating diffuse auroras. Furthermore, a few studies showed that TDSs can efficiently scatter less than a few keV electrons into the loss cone, thereby contributing to the diffuse auroral precipitation (Shen et al., 2020, 2021; Vasko et al., 2017, 2018).

Although individual conjunction events have revealed moderate correlations between TDSs and diffuse auroras (see Supporting Information in Shen et al., 2020), and their similar statistical distributions in the nightside plasma sheet lend support (Malaspina et al., 2015; Newell et al., 2009), direct evidence remains elusive.

Prior statistical studies revealed that TDSs are abundant in the plasma sheet within most plasma injections and braking fast ion flows or bursty bulk flows (BBFs) (Angelopoulos et al., 1992; Ergun et al., 2015; Gurnett & Frank, 1977; Malaspina et al., 2015). These fast ion flows often manifest in the ionosphere as north–south auroral structures or “streamers” (e.g., Henderson, 2012; Lyons et al., 2012; Nishimura et al., 2011). Auroral streamers are typically discrete in nature and are linked to upward field-aligned currents forming on the western edge of flow bursts (Nakamura et al., 2001; Nishimura et al., 2011). However, some streamers may coexist with or evolve into diffuse aurora enhancements as they move equatorward and reach the inner edge of the plasma sheet (Henderson et al., 1998). Within the braking flows, TDSs may contribute to electron precipitation into structured diffuse and non-accelerated auroras (Sergeev et al., 2004; Shen et al., 2020).

Low-energy ($< \sim 1$ keV) electron precipitation more effectively excites red-line (630 nm) auroras, whereas higher-energy (> 1 keV) electrons predominantly induce green-line (557.7 nm) and blue-line (427.8 nm) auroras (Liang et al., 2016; Paschmann et al., 2002). Thus, TDSs are likely linked to red-line-dominated auroras, especially when the plasma sheet state is prime for such low-energy precipitation, like quiet times with low temperatures. In fact, to reliably identify TDS-driven diffuse auroras, non-substorm conditions are more suitable, as it is often challenging to disentangle aggregated effects from different, concurrent drivers during substorms that preclude direct linkage to flow bursts and TDSs (e.g., Sergeev et al., 2012; Shen et al., 2023).

One potential example has been reported by Liang et al. (2011), where conjugate THEMIS and ground-based optical and radar observations revealed flow-related auroral signatures, including red-line diffuse-like auroras that are associated with discrete forms. In that study, THEMIS waveform data and potential TDS signatures have not been investigated, leaving the impact of TDS-induced electron scattering on red-line auroras unresolved. In this paper, we revisit this event, aiming to provide the first forward modeling and data-model comparison of red-line diffuse auroras driven by TDSs.

2. Instrumentation and Models

We use the following data from THEMIS (Angelopoulos, 2008): electron and ion fluxes and moments measured by the Electrostatic Analyzers (ESA) and the Solid State Telescope (SST) instruments in the energy range of several eV up to 900 keV (Angelopoulos et al., 2008; McFadden et al., 2008), DC vector magnetic fields at spin resolution (~ 3 s) measured by the Fluxgate Magnetometers (FGM) (Auster et al., 2008), electric and magnetic field wave power spectra within 1 Hz–4 kHz (FBK with 6 frequency bands and FFP with 64 bands), and waveform data at 8,192 samples per second (sps, DC-coupled), measured by the Electric Field Instrument (EFI), the search coil magnetometer (SCM), and the Digital Fields Board (DFB) (Bonnell et al., 2008; Cully et al., 2008; Le Contel et al., 2008).

The flow-related red-line auroral event occurred during 10:30–11:30 UT on 3 March 2009. Following Liang et al. (2011), we primarily use the ground-based Poker Flat meridian spectrograph (PFMSP) for auroral observations, recording every 15 s and capturing emissions in the red (630 nm), green (557.7 nm), blue (427.8 nm), and proton H_{β} (486.1 nm) lines along the meridian. Complementarily, the Poker Flat digital all-sky camera (DASC) provided 2D auroral data to elucidate the longitudinal or magnetic local time (*MLT*) extent of the red-line diffuse auroras. Note that the DASC does not provide absolute intensities of 630 nm emissions and it recorded images at 41-s cadence for this event. We also use auroral observations from the THEMIS whitelight all-sky imager (ASI) at Fort Yukon with 3-s cadence (Mende et al., 2008).

Although TDSs include different types of nonlinear electrostatic structures as noted by Mozer et al. (2015), electron phase space holes are the predominant type in the near-Earth plasma sheet (e.g., Ergun et al., 2015; Malaspina et al., 2018). Electron scattering by electron holes can be quantified using the quasi-linear approach initially developed for an ensemble of plane waves (Kennel & Engelmann, 1966; Lyons, 1974), assuming statistically uniform, stationary, and weak TDS turbulence and electron random gyro-phases during interactions (Vasko et al., 2018). We use the formulation of local pitch-angle diffusion coefficients $D_{\alpha\alpha}$ derived in Vasko et al. (2018) and refined by Shen et al. (2021). We bounce average the local diffusion rates using the standard procedure (Glauert & Horne, 2005; Lyons et al., 1972):

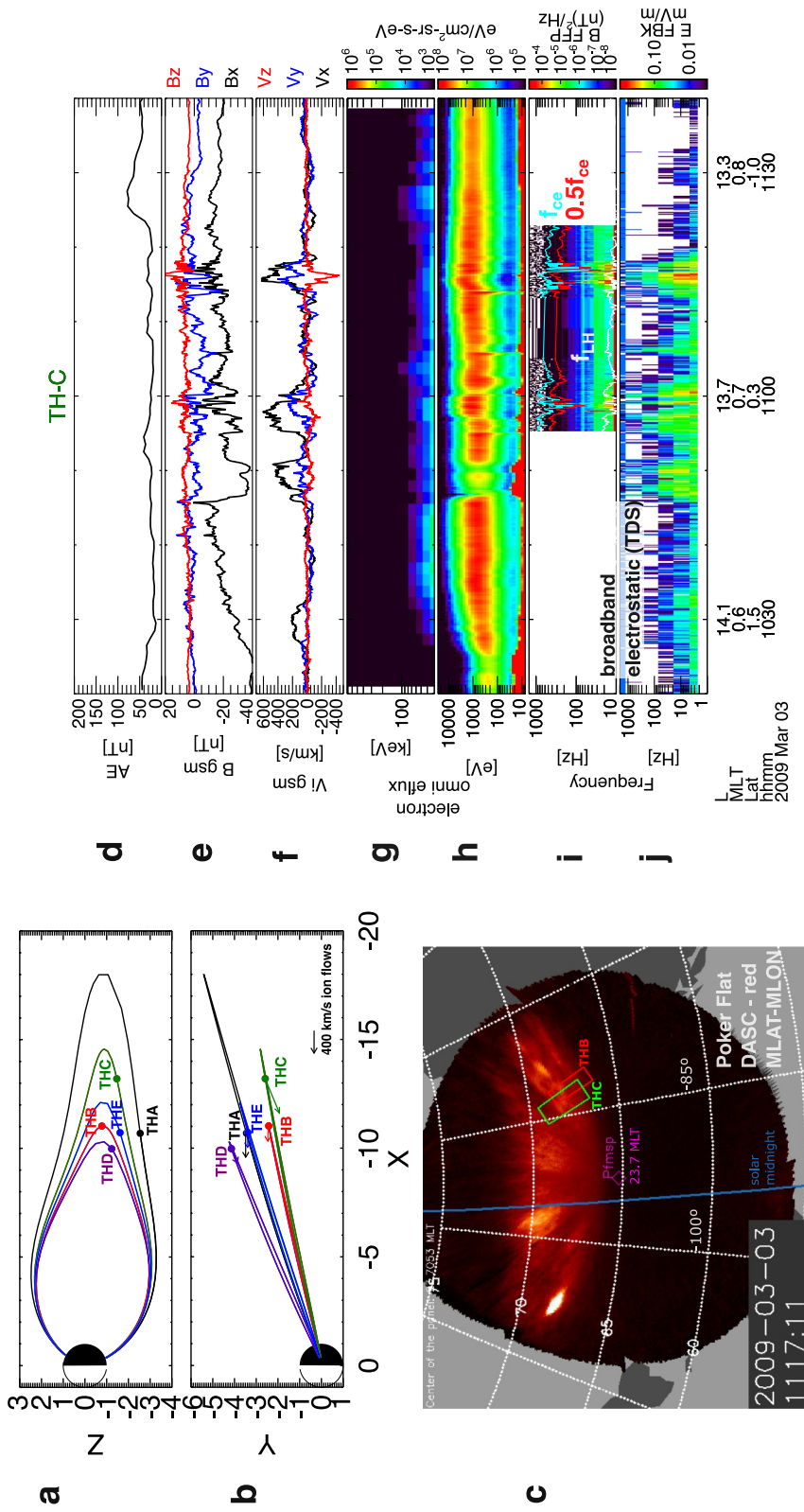


Figure 1. Overview of the flow-related red-line diffuse aurora event observed by THEMIS-C and Poker Flat all-sky camera (DASC). (a, b) Field line configuration threading the five THEMIS spacecraft in the GSM coordinates. Colored vectors represent ion flow velocities for each spacecraft. (c) Poker Flat DASC red-line auroras measured near 11:17 UT. The grids represent AACGM magnetic latitude and magnetic longitude, while the blue line marks the actual local midnight. The assumed emission height and approximate footprints of THEMIS-B (red box), THEMIS-C (green box), and Poker Flat have been mapped to ~200 km altitude using different Tsyganenko models of T89, T96, and T01. (d) THEMIS AE index. (e) Magnetic fields. (f) Ion flow velocities. (g, h) Electron energy spectrum from 7 eV up to 900 keV. (i) Magnetic field FBK spectra in 10 Hz–2 kHz. (j) Electric field FBK spectra up to 2 kHz.

$$\langle D_{\alpha_{eq}\alpha_{eq}} \rangle = v^{-1} \tau_B^{-1} \int_{\lambda_{m,south}}^{\lambda_{m,north}} D_{\alpha\alpha} (\partial \alpha_{eq} / \partial \alpha)^2 (\partial s / \partial \lambda) d\lambda / \cos \alpha, \quad (1)$$

where the integration is over the period of bounce motion τ_B , between the south and north mirror points $\lambda_{m,south}$ and $\lambda_{m,north}$, and $s = s(\lambda)$ is the length of a field line. We use the relatively realistic T89 magnetic field model for bounce-averaging (Ma et al., 2012; Tsyganenko, 1989). We modify the latitudinal profile of \mathbf{B} near the equator using a spline function fit to match the locally measured \mathbf{B} by THEMIS. As a result, the magnetic field stretching is reduced near the equator (e.g., Ni et al., 2012). In addition, bounce-averaged pitch angle diffusion coefficients due to transient whistler-mode waves are also calculated using the Full Diffusion Code (Ma et al., 2020; Ni et al., 2008), including the Landau ($n = 0$) and higher order (n up to ± 10) cyclotron harmonic resonances.

We use the full precipitating electron distributions calculated from quasilinear diffusion theory to forward model TDS-driven red-line auroras. Because the varying timescale of precipitation is typically shorter than the radiative timescale (~ 110 s) of 630 nm emission, it is imperative to use a time-dependent auroral transport code, such as the TREx-ATM model (Liang et al., 2016). TREx-ATM is a time-dependent ionosphere aurora model, adopting the two-stream electron transport code embedded in the GLOW model (Solomon et al., 1988) and ambipolar diffusion to compute the electron transport in the atmosphere, with additional capabilities to compute the impact ionization, secondary electron production, and impact excitation of neutrals.

3. Results

The event featuring bursty bulk flows and red-line auroras was observed from 10:40 to 11:20 UT on 3 March 2009. During this time, THEMIS-C spacecraft detected a series of high-speed flow bursts (>400 km/s) in the Earth's plasma sheet, as shown in Figure 1. Figures 1a–1c illustrate the magnetic fields threading all five THEMIS spacecraft, modeled by T89, alongside the 2D ionospheric red-line auroras observed by Poker Flat DASC. The red-line auroras spanned nearly 45° in magnetic longitude or 3 hr in *MLT*, primarily drifted eastward, occasionally moving equatorward, and exhibited both diffuse-like and discrete enhancements.

For this event complementary ground-based measurements, including THEMIS ASIs and Poker Flat incoherent scatter radar, provided synergistic auroral and ionospheric density observations as detailed by Liang et al. (2011). While not described again here, the key findings include: (a) flow-related auroras featured intermittent poleward boundary intensifications (PBIs) and streamer-like green line emissions, occasionally coinciding with or transitioning to predominantly red-line diffuse-like auroras at lower latitudes; (b) ionospheric density altitude profiles were consistent with the red-line emissions and soft (<1 keV) electron precipitation; (c) southward-moving density patches corresponded to earthward flow bursts and red-line auroral enhancements. It was noted that the absence of substantial density enhancements above 200 km and the latitudinally extended red-line diffuse-like emissions were inconsistent with typical small-scale Alfvénic auroras and broadband acceleration (Chaston et al., 2003; Liang et al., 2019). However, for some observed discrete auroras, such as the bright stripes around -100° magnetic longitude and discrete structures near the poleward boundary (likely linked to PBIs) in Figure 1c, Alfvénic acceleration cannot be ruled out (Damiano et al., 2015; Hull et al., 2022; Tian et al., 2021), though these aspects are not the main focus of this study. Auroral features will be further examined using multi-spectra PFMSF measurements.

Figures 1b and 1c indicate that of the five THEMIS spacecraft, THB and THC were closest to midnight, with their footprints less than 1 hr *MLT* east of Poker Flat. THC detected all flow bursts exceeding 400 km/s within BBFs, whereas THB, positioned further earthward, registered only a weaker flow burst (~ 200 km/s) that had waned during inward propagation. Figure 1d shows that the *AE* index remained below 80 nT throughout the event. Three strong flow bursts were recorded between 10:40 and 11:20 UT, each lasting ~ 5 min. The latter two, occurring closer to the equator, were accompanied by $|B_x|$ decreases, notable B_z dipolarizations (Figure 1e), and slightly energized electron spectra (Figure 1h). Despite heightened flow activity, the plasma sheet temperature remained below 1 keV (Liang et al., 2011). Figures 1i and 1j show that the flow bursts corresponded to enhanced broadband electrostatic fluctuations (or TDSs) with frequencies ranging from tens of Hz to several kHz. Additionally, sporadic electromagnetic wave power enhancements, mostly below ~ 20 Hz, indicate the presence of kinetic Alfvén waves (KAWs) (e.g., Chaston et al., 2012; Malaspina et al., 2018; Shen et al., 2023).

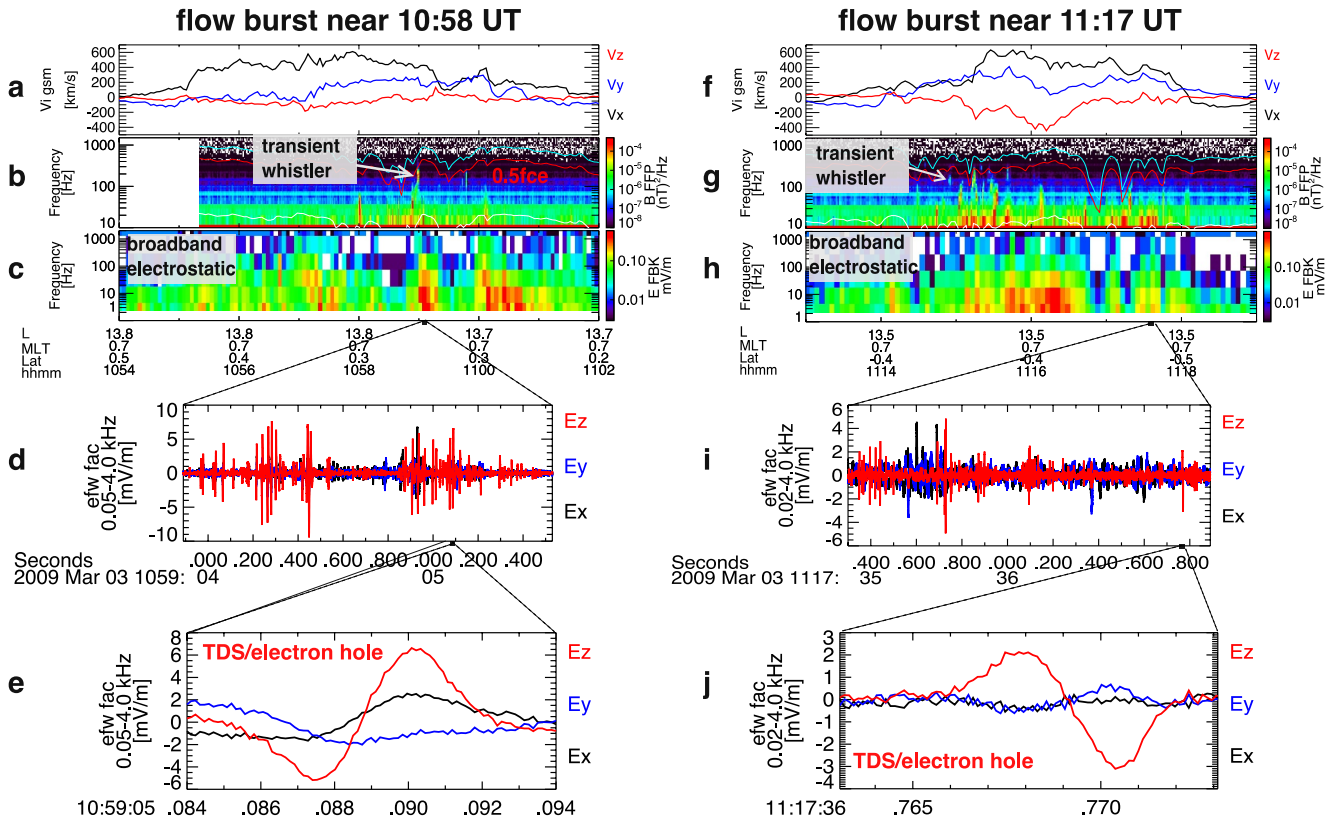


Figure 2. Zoomed-in view of the plasma waves within the two flow bursts near 10:58 UT (a–e) and 11:17 UT (f–j). Panels from top to bottom are: ion flow velocities, FFP magnetic field spectra, FBK electric field spectra, waveform measurements of high-frequency (>20 Hz and >50 Hz) electric fields in the field-aligned coordinates (**B** is in the z direction), and expanded views of millisecond-scale electron phase-space holes, also known as time-domain structures (TDSs).

Figure 2 provides a detailed view of wave spectra and waveform measurements associated with two flow bursts near 10:58 UT and 11:17 UT. Throughout the flow intervals, there were continuous enhancements in broadband electrostatic fluctuations. Figures 2d, 2e, 2i, and 2j clearly show that these broadband electrostatic fluctuations predominantly consisted of electron phase-space holes, identified by bipolar parallel (in the z direction) and unipolar perpendicular (in the x and y direction) electric fields on the timescales of millisecond or on the spatial scales of the local Debye length (Hutchinson, 2017; Lotekar et al., 2020; Muschietti et al., 1999). In contrast, whistler-mode waves were more ephemeral, characterized by sporadic, narrow-band magnetic power enhancements lasting less than 1 minute within the flow intervals (Figures 2b and 2g).

Based on the observed characteristics of TDSs and whistler-mode waves, we proceed to calculate bounce-averaged electron pitch-angle diffusion rates $\langle D_{\alpha_{eq}\alpha_{eq}} \rangle$ and resulting electron distributions precipitating into the ionosphere (Ma et al., 2012, 2020; Shen et al., 2021). For TDSs, local diffusion coefficients do not depend on individual electron hole electric fields, but on the root-mean-square intensity E_w derived from spectra data, which take into account the occurrence of electron holes (Shen et al., 2021; Vasko et al., 2018). Following Shen et al. (2021), we also adapt statistical electron hole velocity and parallel scale distributions based on the local plasma parameters for diffusion rate calculations. TDSs can be generated locally at various latitudes and continuously along the propagation of flow bursts and injections toward Earth (Ergun et al., 1998; Franz et al., 2005; Malaspina et al., 2015; Mozer et al., 2015). We assume a latitudinal distribution of electron holes to be within $\pm 25^\circ$ near the equator (Shen et al., 2021; Vasko et al., 2017); increasing the latitude extent to $\pm 45^\circ$ enhances the diffusion rate near the loss cone by <20%.

For transient whistler-mode waves, we determine the average wave spectra near 11:15 UT (Figure 2g) as having a Gaussian with a lower limit $\omega_1 = 0.15\Omega_{ce}$, a mean frequency $\omega_2 = 0.3\Omega_{ce}$, an upper limit $\omega_m = 0.45\Omega_{ce}$, a bandwidth $\delta\omega = 0.075\Omega_{ce}$, and a mean wave amplitude $B_w = 50$ pT. No whistler-mode waves were measured by waveform data in our event, thus we do not have direct information on their wave normals. For the nightside

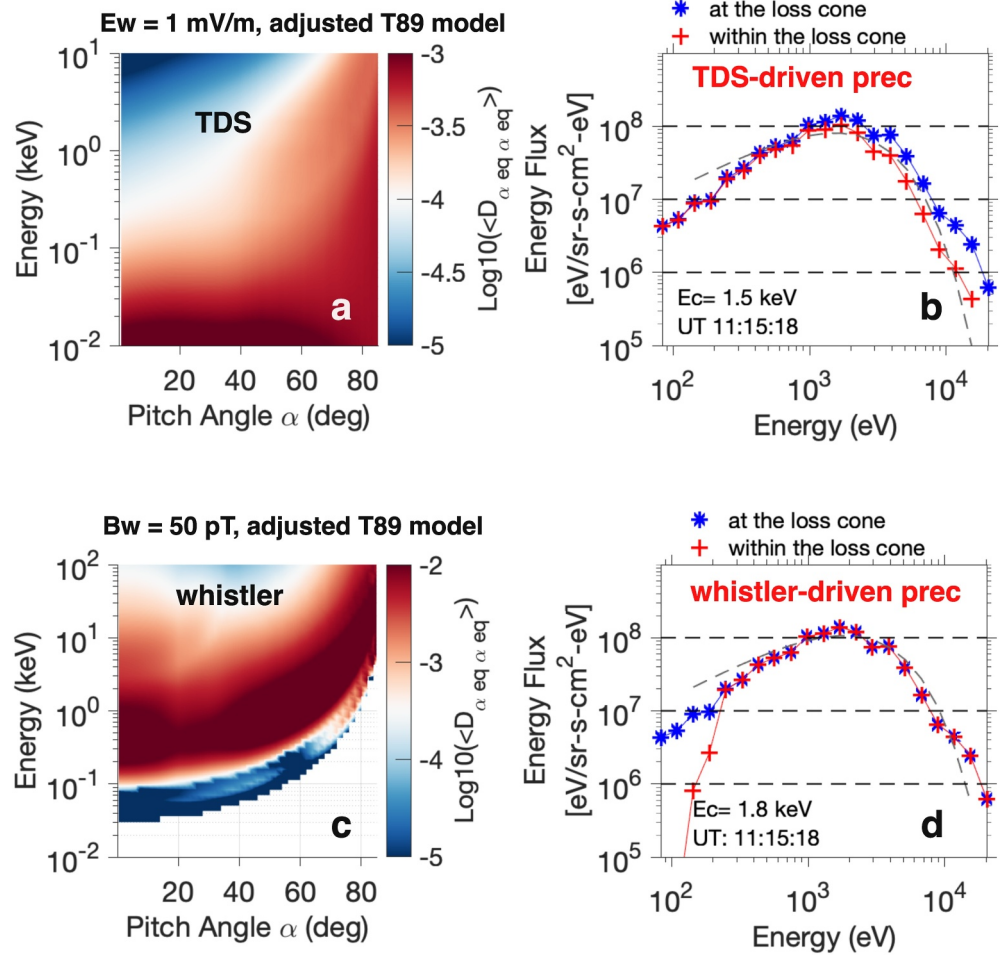


Figure 3. (a, c) TDS- and whistler-driven bounce-averaged electron pitch-angle diffusion rates ($\langle D_{\alpha_{eq}\alpha_{eq}} \rangle$) as a function of energy and pitch angle. We use adjusted T89 model for bounce averaging. (b, d) Example energy flux distributions extrapolated to the loss cone (blue) and calculated within the loss cone (red) based on $\langle D_{\alpha_{eq}\alpha_{eq}} \rangle$. The gray-dashed curves indicate Maxwellian fittings of the precipitating distributions due to TDSs and whistlers, indicating characteristic energies of 1.5 and 1.8 keV near 11:15:18 UT.

equatorial plasma sheet (Agapitov et al., 2013; Li et al., 2011; Meredith et al., 2021), we can assume parallel whistlers confined within $\pm 15^\circ$ latitude near the equator, having Gaussian wave normals with a width $\theta_w = 10^\circ$, a minimum $\theta_{min} = 0^\circ$, and a maximum $\theta_{max} = 30^\circ$. We set the background $n_e \sim 0.6 \text{ cm}^{-3}$, $f_{pe}/f_{ce} \sim 14.4$, and $L \sim 14.0$ based on THEMIS observations. For bounce averaging, we use the T89 model with slight adjustments near the equator to align with THEMIS-C local B observations. Applying different magnetic field models, such as T96 and T01, we have obtained variations of less than a factor of 2 in $\langle D_{\alpha_{eq}\alpha_{eq}} \rangle$ near the loss cone for TDS and whistler-mode waves (Ma et al., 2012), which further translates to a variation in precipitating flux of less than 40%.

Figures 3a and 3c present the calculated $\langle D_{\alpha_{eq}\alpha_{eq}} \rangle$ as a function of energy and pitch angle, resulting from electron scattering by TDSs and whistler-mode waves, respectively. Near the loss cone ($\sim 1^\circ$), TDSs efficiently induce pitch-angle scattering at energies below a few keV, with $\langle D_{\alpha_{eq}\alpha_{eq}} \rangle$ on the order of 10^{-4} – 10^{-3} s^{-1} , assuming $E_w \sim 1 \text{ mV/m}$, compared with the strong diffusion limit of $D_{sd} \sim 10^{-5} \text{ s}^{-1}$ at $L \sim 14.0$ (Kennel & Petschek, 1966). At any instance during the event, we may obtain $\langle D_{\alpha_{eq}\alpha_{eq}} \rangle$ by multiplying a factor of E_w^2 based on quasilinear theory (Kennel & Engelmann, 1966; Vasko et al., 2018). Due to large f_{pe}/f_{ce} for this event, whistler-mode waves can also drive efficient electron scattering at energies as low as 200 eV, but the scattering rates exhibit a broad

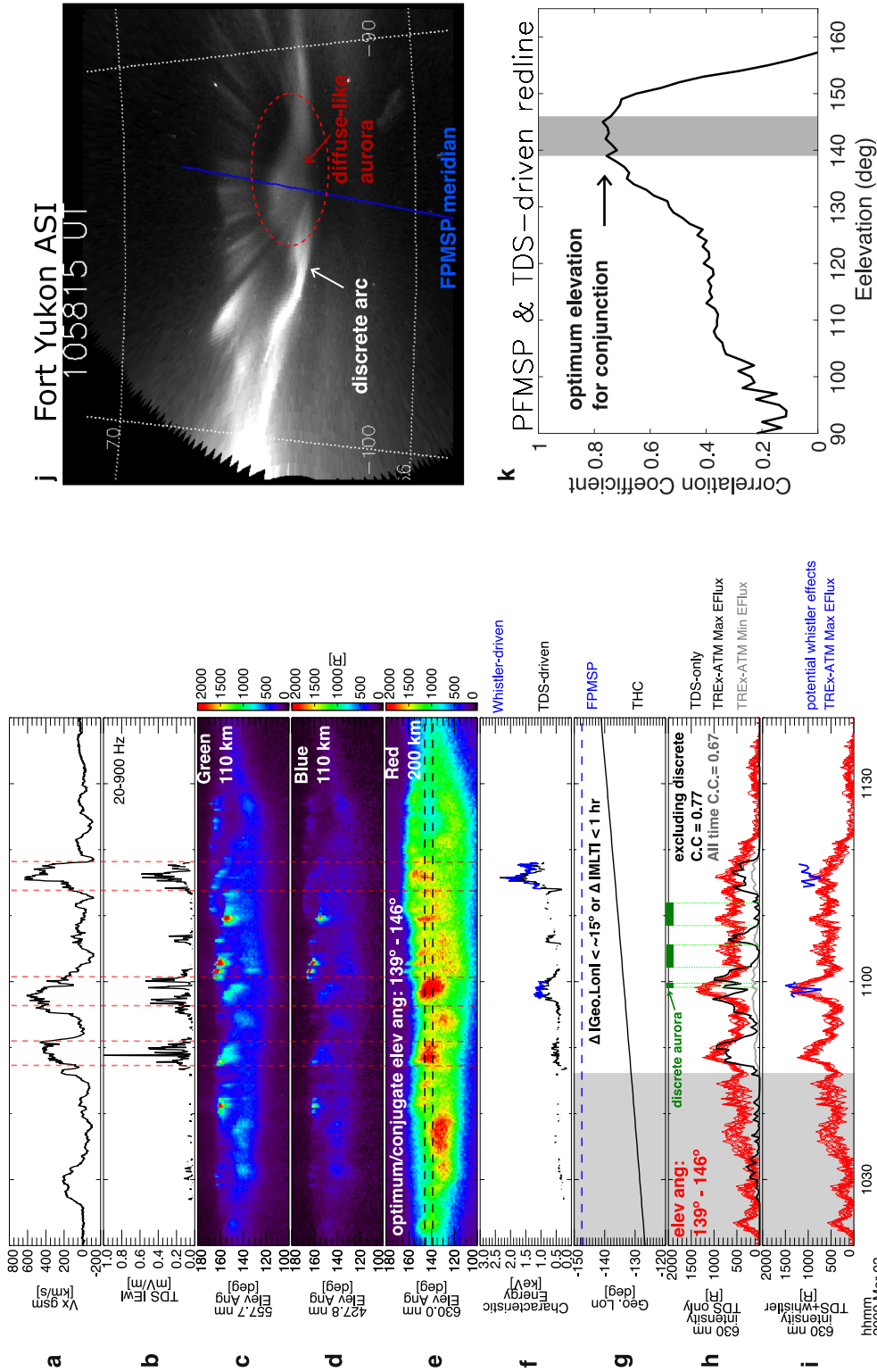


Figure 4. Auroral features and TREx-ATM model results. (a) Ion flow velocity V_x . (b) Root-mean-square TDS electric field amplitudes $|E_w|$ (20–900 Hz). (c–e) PFMSP 557.7-nm green-line, 427.8-nm blue-line, and 630-nm red-line intensity; dashed lines mark optimal elevation angle range for THEMIS conjunction. (f) Characteristic energies of electrons precipitated by TDS (black) and whistler-mode waves (blue). (g) Geographic longitudes of PFMSP and THEMIS-C footprints. (h) 630-nm intensity: PFMSP data (red) versus TDS-driven TREx-ATM model results (black, gray) based on THEMIS maximum and minimum fluxes around the equator (see Supporting Information S1). (i) TREx-ATM results with additional inputs from assumed, persistent whistler-mode waves; only maximum electron fluxes used. (j) Example ASI whitelight image showing diffuse-like auroras near PFMSP that likely evolved from discrete auroras at various elevation angles.

peak near 1 keV, extending up to 100 keV. This suggests that whistler-mode waves tend to produce more energetic precipitation spectra compared with TDSs.

Example precipitating electron energy distributions are shown in Figures 3b and 3d. The differential energy flux (red pluses) within the loss cone can be estimated as $x(E)J(E, \alpha_{LC})$, where

$$x(E) = 2 \int_0^1 I_0(Z_0 \tau) \tau d\tau / I_0(Z_0), \quad (2)$$

being the index of loss cone filling, $J(E, \alpha_{LC})$ is the electron differential energy flux at the edge of the loss cone ($\sim 1^\circ$, blue stars), I_0 is the modified Bessel function with an argument $Z_0 \simeq \alpha_{LC} / \sqrt{\langle D_{aa} \rangle_{LC} \cdot \tau_{loss}}$ (Kennel & Petschek, 1966), and τ_{loss} is assumed to be half of the bounce period.

Simultaneously measured time-varying precipitating electron full distributions are input into the time-dependent TREx-ATM code to forward model red-line auroras and compare their evolution with that of the measured red-line diffuse-like auroras by PFMSAP. We begin by examining PFMSAP auroral observations. Figures 4a–4d display approximately correlated ion flow bursts, TDS E_w , and enhanced auroral activities in the green line (577.7 nm), blue line (427.8 nm), and red line (630 nm). To obtain wave amplitudes of TDSs from FBK spectra (Figure 2), we integrate wave power in the frequency range of 20–900 Hz, as informed by TDS wavelet analyses (Shen et al., 2021). The flow bursts (>400 km/s) were associated with intermittent poleward boundary intensifications (PBIs) near 160° elevation angle (or $\sim 68^\circ$ magnetic latitudes) in the green and blue line emissions, exhibiting distinct equatorward movement. These features align with auroral streamers associated with earthward flow channels in the plasma sheet (e.g., Henderson, 2012; Lyons et al., 2012; Nishimura et al., 2011).

However, the majority of the auroral enhancements were noted in the red line, predominantly equatorward of the green-line enhancements. These enhanced red-line emissions, characterized by “patchiness” or short-lived activations, coincided with TDS amplitude increases and exhibited discernible equatorward movement. As noted by Liang et al. (2011), this movement was also in accord with the equatorward shift of soft electron precipitation and enhanced density patches at altitudes above 150 km. Figure 4f suggests that TDS-driven precipitation has characteristic energies mostly below 1 keV, consistent with the overwhelmingly red-line emissions and soft electron precipitation. In contrast, assuming the presence of whistler-mode waves throughout the flow bursts near 10:58 UT and 11:17 UT, these would produce precipitation with characteristic energies exceeding 1 keV.

To compare with TREx-ATM model output, we need to identify PFMSAP red-line diffuse-like aurora intensifications that were approximately conjugate with THEMIS observations. First, we focus on the time interval between 10:45 and 11:30 UT, during which the longitudinal separation between the PFMSAP meridian and projected THEMIS-C footprints was less than 15° , or equivalently $|\Delta MLT| < 1$ hr (Figure 4g). Second, we adjust the PFMSAP red-line data counts by subtracting a uniform background attributed to ambient diffuse auroras, likely arising from non-TDS mechanisms like diffuse proton precipitation (e.g., Lyons et al., 2015) as indicated by PFMSAP H_β -line emissions. Third, after applying Van Rhijin correction to data counts for aspect angle effects, we identify an optimum range of elevation angles of 139° – 146° , which probably corresponded to THEMIS measurements. These optimal angles were determined by searching the maximum correlation coefficients between the modeled and observed red-line emissions across all elevation angles (Figure 4k).

The event exhibited coexisting auroral types due to various mechanisms. TDS-induced soft electron precipitation leads to a broader altitude distribution of both 630 and 577.7 nm emissions, unlike the narrow altitude range associated with monoenergetic electron acceleration in discrete arcs. In oblique optical observations, like those from PFMSAP and THEMIS ASI, this broader distribution may appear as more “diffusive” auroral forms (see Figure 4j around the PFMSAP meridian). Additional ASI auroral images are provided in Supporting Information S1. The 630-nm emission in our event, particularly sensitive to soft electron precipitation, aligns closely with TDS effects. We have carefully examined the observations from the Fort Yukon ASI (see Supporting Movie in Liang et al. (2011)) and excluded three periods when discrete arcs predominately contribute to PFMSAP red-line emissions.

Figure 4h shows a correlation coefficient of 0.77 between PFMSAP observed and TREx-ATM forward-modeled red-line emissions, using inputs solely from TDS-driven precipitation. The TREx-ATM model results, indicated by the black and gray lines, are based on maximum and minimum flux levels measured by THEMIS near the

equator during 10:40–11:20 UT. These in-situ measured fluxes were largely controlled by the spacecraft's proximity to the true equator, where $|B_x|$ is minimum (see Supporting Information S1). Figure 4h reveals that the majority of the observed red-line diffuse-like auroral enhancements during flow bursts can be explained by TDS-driven model results, albeit slightly underestimated for the most intense emissions. Green bars highlight the time intervals of discrete emission peaks, unrelated to TDSs, near 11:00, 11:05, and 11:10 UT. Including these intervals in our analysis lowers the correlation to 0.67. Figure 4i suggests that including potential whistler-mode wave effects along with TDSs in the model offers a better explanation for the two bright red spots near 10:58 UT and 11:17 UT. This implies that whistler-mode waves might also contribute to the most intense red-line diffuse emissions during flow bursts. The compound effects of whistler-mode waves and field-aligned acceleration on energetic electron precipitation obscure TDS's role in 557.7-nm emissions. Nonetheless, we have analyzed TDS-driven TREx-ATM 557.7-nm outputs and observed a weaker correlation with PFMSP's green line (~ 0.6).

4. Discussion

Plasma sheet flow bursts are typically linked to ionospheric auroral PBIs and equatorward-moving auroral streamers, as evidenced by white-light all-sky imager (ASI) observations, often around substorm times (Donovan et al., 2008; Forsyth et al., 2020; Nishimura et al., 2011; Yadav et al., 2022). In our non-substorm event, while green-line PBIs and forms resembling equatorward-moving auroral streamers were noted, the most prominent feature was the red-line auroras. These auroras extended toward lower latitudes and often appeared more diffuse than discrete near PFMSP, likely due to wave scattering. Liang et al. (2011) suggests that the predominance of red-line emissions was probably due to a cooler inner plasma sheet ($T_e < \sim 1$ keV). Despite strong flows and potential association with hot electrons in the tail leading to streamer-inducing energetic precipitation (Angelopoulos et al., 1992; Nishimura et al., 2020), there was an absence of significant energetic injections intruding the inner plasma sheet around midnight (Figure 1g). This could be attributed to differences in adiabatic motion or Alfvén layers between soft and energetic electrons as they undergo convective, curvature and gradient drifts during inward propagation (e.g., Gabrielse et al., 2017).

While red-line emissions naturally accompany green-line emissions due to the $O(^1S)$ to $O(^1D)$ transition linked with 557.7 nm photo emission (Solomon et al., 1988), the dominance of red-line auroral emissions indicates a major low-energy precipitation population, distinct from the energetic precipitation responsible for green line excitation. This low-energy precipitation was confirmed by ionospheric density altitude profiles measured by PFISR (Liang et al., 2011). During the event period of our interest, ECH waves were not observed, ruling them out as a cause for the auroral precipitation (Ni et al., 2012; Zhang et al., 2015). Our investigations point to electron scattering by TDSs as the primary driver of the observed low-energy precipitation and red-line diffuse-like auroras.

5. Conclusion

This letter revisits a flow-related red-line aurora event initially reported by Liang et al. (2011). Analyzing THEMIS spectra and waveform measurements, we have revealed an abundance of time-domain structures (TDSs) associated with magnetotail flow bursts. Applying quasilinear calculations, we have estimated TDS-driven electron distributions precipitating into the ionosphere. Employing the time-dependent TREx-ATM auroral transport code, we have forward-modeled red-line auroras due to TDS-driven precipitation. The good correlation of ~ 0.77 between modeled and observed red-line emissions suggests that TDSs likely cause the observed red-line diffuse-like auroras, which sometimes coexisted with or likely evolved from discrete forms. However, to fully explain the most intense red-line emissions, contributions from whistler-mode waves are also necessary. Our study suggests that wave-driven red-line diffuse auroras, associated with braking flow bursts, offer a distinct yet complementary pathway of MI-coupling compared with well-established flow-driven discrete auroral streamers, typically seen in the green line and caused by field-aligned potential acceleration.

Data Availability Statement

THEMIS data is available at <http://themis.ssl.berkeley.edu/data/themis/>. Poker Flat DASC and MSP can be accessed at <http://optics.gi.alaska.edu/optics/?q=archive>. The bounce-averaged pitch-angle diffusion rates shown

in Figure 3 are available through the Zenodo archive at <https://doi.org/10.5281/zenodo.11044554> (Shen, 2024). Data access and processing was done using SPEDAS V4.1, see Angelopoulos et al. (2019).

Acknowledgments

This work has been supported by NASA projects 80NSSC23K0413, 80NSSC23K0108, 80NSSC22K1638, and 80NSSC20K1325. Q.M. acknowledges the NASA Grant 80NSSC20K0196 and NSF Grant AGS-2225445. L.L. acknowledges the NSF Grant 2055192. J.L. acknowledges the NASA Grants 80NSSC22K0749, 80NSSC22K0751, and NSF Grant AGS-2247034. TREX-ATM is supported by Canadian Space Agency. We thank Jasper Laca for help with editing. We acknowledge the support of NASA contract NAS5-02099 for the use of data from the THEMIS Mission.

References

- Agapitov, O. V., Artemyev, A., Krasnoselskikh, V., Khotyaintsev, Y. V., Mourenas, D., Breuillard, H., et al. (2013). Statistics of whistler mode waves in the outer radiation belt: Cluster STAFF-SA measurements. *Journal of Geophysical Research*, *118*(6), 3407–3420. <https://doi.org/10.1002/jgra.50312>
- Angelopoulos, V. (2008). The THEMIS mission. *Space Science Reviews*, *141*(1–4), 5–34. <https://doi.org/10.1007/s11214-008-9336-1>
- Angelopoulos, V., Baumjohann, W., Kennel, C. F., Coronti, F. V., Kivelson, M. G., Pellat, R., et al. (1992). Bursty bulk flows in the inner central plasma sheet. *Journal of Geophysical Research*, *97*(A4), 4027–4039. <https://doi.org/10.1029/91JA02701>
- Angelopoulos, V., Cruce, P., Drozdov, A., Grimes, E. W., Hatzigeorgiu, N., King, D. A., et al. (2019). The Space Physics Environment Data Analysis System (SPEDAS). *Space Science Reviews*, *215*(1), 9. <https://doi.org/10.1007/s11214-018-0576-4>
- Angelopoulos, V., Sibeck, D., Carlson, C. W., McFadden, J. P., Larson, D., Lin, R. P., et al. (2008). First results from the THEMIS mission. *Space Science Reviews*, *141*(1–4), 453–476. <https://doi.org/10.1007/s11214-008-9378-4>
- Auster, H. U., Glassmeier, K. H., Magnes, W., Aydogar, O., Baumjohann, W., Constantinescu, D., et al. (2008). The THEMIS fluxgate magnetometer. *Space Science Reviews*, *141*(1–4), 235–264. <https://doi.org/10.1007/s11214-008-9365-9>
- Bonnell, J. W., Mozer, F. S., Delory, G. T., Hull, A. J., Ergun, R. E., Cully, C. M., et al. (2008). The Electric Field Instrument (EFI) for THEMIS. *Space Science Reviews*, *141*(1–4), 303–341. <https://doi.org/10.1007/s11214-008-9469-2>
- Cattell, C., Dombek, J., Wygant, J., Drake, J. F., Swisdak, M., Goldstein, M. L., et al. (2005). Cluster observations of electron holes in association with magnetotail reconnection and comparison to simulations. *Journal of Geophysical Research*, *110*(A1), 1211. <https://doi.org/10.1029/2004JA010519>
- Chaston, C. C., Bonnell, J. W., Clausen, L., & Angelopoulos, V. (2012). Energy transport by kinetic-scale electromagnetic waves in fast plasma sheet flows. *Journal of Geophysical Research*, *117*(A9), 9202. <https://doi.org/10.1029/2012JA017863>
- Chaston, C. C., Peticolas, L. M., Bonnell, J. W., Carlson, C. W., Ergun, R. E., McFadden, J. P., & Strangeway, R. J. (2003). Width and brightness of auroral arcs driven by inertial Alfvén waves. *Journal of Geophysical Research*, *108*(A2), 1091. <https://doi.org/10.1029/2001JA007537>
- Cully, C. M., Ergun, R. E., Stevens, K., Nammari, A., & Westfall, J. (2008). The THEMIS digital fields board. *Space Science Reviews*, *141*(1–4), 343–355. <https://doi.org/10.1007/s11214-008-9417-1>
- Damiano, P. A., Johnson, J. R., & Chaston, C. C. (2015). Ion temperature effects on magnetotail Alfvén wave propagation and electron energization. *Journal of Geophysical Research*, *120*(7), 5623–5632. <https://doi.org/10.1002/2015JA021074>
- Donovan, E., Liu, W., Liang, J., Spanswick, E., Voronkov, I., Connors, M., et al. (2008). Simultaneous THEMIS in situ and auroral observations of a small substorm. *Geophysical Research Letters*, *35*(17), L17S18. <https://doi.org/10.1029/2008GL033794>
- Ergun, R. E., Carlson, C. W., McFadden, J. P., Mozer, F. S., Delory, G. T., Peria, W., et al. (1998). FAST satellite observations of large-amplitude solitary structures. *Geophysical Research Letters*, *25*(12), 2041–2044. <https://doi.org/10.1029/98GL00636>
- Ergun, R. E., Goodrich, K. A., Stawarz, J. E., Andersson, L., & Angelopoulos, V. (2015). Large-amplitude electric fields associated with bursty bulk flow braking in the Earth's plasma sheet. *Journal of Geophysical Research*, *120*(3), 1832–1844. <https://doi.org/10.1002/2014JA020165>
- Forsyth, C., Sergeev, V. A., Henderson, M. G., Nishimura, Y., & Gallardo-Lacourt, B. (2020). Physical processes of Meso-Scale, dynamic auroral forms. *Space Science Reviews*, *216*(4), 46. <https://doi.org/10.1007/s11214-020-00665-y>
- Franz, J. R., Kintner, P. M., Pickett, J. S., & Chen, L.-J. (2005). Properties of small-amplitude electron phase-space holes observed by Polar. *Journal of Geophysical Research*, *110*(A9), A09212. <https://doi.org/10.1029/2005JA011095>
- Gabrielse, C., Angelopoulos, V., Harris, C., Artemyev, A., Kepko, L., & Runov, A. (2017). Extensive electron transport and energization via multiple, localized dipolarizing flux bundles. *Journal of Geophysical Research*, *122*(5), 5059–5076. <https://doi.org/10.1002/2017JA023981>
- Glauert, S. A., & Horne, R. B. (2005). Calculation of pitch angle and energy diffusion coefficients with the PADIE code. *Journal of Geophysical Research*, *110*(A4), 4206. <https://doi.org/10.1029/2004JA010851>
- Gurnett, D. A., & Frank, L. A. (1977). A region of intense plasma wave turbulence on auroral field lines. *Journal of Geophysical Research*, *82*(7), 1031–1050. <https://doi.org/10.1029/JA082i007p01031>
- Gurnett, D. A., Frank, L. A., & Lepping, R. P. (1976). Plasma waves in the distant magnetotail. *Journal of Geophysical Research*, *81*(34), 6059–6071. <https://doi.org/10.1029/JA081i034p06059>
- Henderson, M. G. (2012). Auroral substorms, poleward boundary activations, auroral streamers, omega bands, and onset precursor activity. In *Auroral phenomenology and magnetospheric processes: Earth and other planets* (pp. 39–54). American Geophysical Union (AGU). <https://doi.org/10.1029/2011GM001165>
- Henderson, M. G., Reeves, G. D., & Murphree, J. S. (1998). Are north-south aligned auroral structures an ionospheric manifestation of bursty bulk flows? *Geophysical Research Letters*, *25*(19), 3737–3740. <https://doi.org/10.1029/98GL02692>
- Hull, A. J., Damiano, P. A., Chaston, C. C., Johnson, J. R., & Reeves, G. D. (2022). Electron energization signatures in traveling kinetic Alfvén waves at storm time injection fronts. *Geophysical Research Letters*, *49*(15), e99318. <https://doi.org/10.1029/2022GL099318>
- Hutchinson, I. H. (2017). Electron holes in phase space: What they are and why they matter. *Physics of Plasmas*, *24*(5), 055601. <https://doi.org/10.1063/1.4976854>
- Kennel, C. F., & Engelmann, F. (1966). Velocity space diffusion from weak plasma turbulence in a magnetic field. *Physics of Fluids*, *9*(12), 2377–2388. <https://doi.org/10.1063/1.1761629>
- Kennel, C. F., & Petschek, H. E. (1966). Limit on stably trapped particle fluxes. *Journal of Geophysical Research*, *71*, 1–28. <https://doi.org/10.1029/jz071i001p00001>
- Le Contel, O., Roux, A., Robert, P., Coillot, C., Bouabdellah, A., de La Porte, B., et al. (2008). First results of the THEMIS search coil magnetometers. *Space Science Reviews*, *141*(1–4), 509–534. <https://doi.org/10.1007/s11214-008-9371-y>
- Li, W., Bortnik, J., Thorne, R. M., & Angelopoulos, V. (2011). Global distribution of wave amplitudes and wave normal angles of chorus waves using THEMIS wave observations. *Journal of Geophysical Research*, *116*(A12), 12205. <https://doi.org/10.1029/2011JA017035>
- Liang, J., Donovan, E., Jackel, B., Spanswick, E., & Gillies, M. (2016). On the 630 nm red-line pulsating aurora: Red-line Emission Geospace Observatory observations and model simulations. *Journal of Geophysical Research: Space Physics*, *121*(8), 7988–8012. <https://doi.org/10.1002/2016JA022901>
- Liang, J., Shen, Y., Knudsen, D., Spanswick, E., Burchill, J., & Donovan, E. (2019). e-POP and red line optical observations of Alfvénic auroras. *Journal of Geophysical Research: Space Physics*, *124*(6), 4672–4696. <https://doi.org/10.1029/2019JA026679>

- Liang, J., Spanswick, E., Nicolls, M. J., Donovan, E. F., Lummerzheim, D., & Liu, W. W. (2011). Multi-instrument observations of soft electron precipitation and its association with magnetospheric flows. *Journal of Geophysical Research*, *116*(A6), 6201. <https://doi.org/10.1029/2010JA015867>
- Lotekar, A., Vasko, I. Y., Mozer, F. S., Hutchinson, I., Artemyev, A. V., Bale, S. D., et al. (2020). Multisatellite mms analysis of electron holes in the Earth's magnetotail: Origin, properties, velocity gap, and transverse instability. *Journal of Geophysical Research: Space Physics*, *125*(9), e2020JA028066. <https://doi.org/10.1029/2020JA028066>
- Lyons, L. R. (1974). Pitch angle and energy diffusion coefficients from resonant interactions with ion-cyclotron and whistler waves. *Journal of Plasma Physics*, *12*(3), 417–432. <https://doi.org/10.1017/S002237780002537X>
- Lyons, L. R., Nishimura, Y., Gallardo-Lacourt, B., Nicolls, M. J., Chen, S., Hampton, D. L., et al. (2015). Azimuthal flow bursts in the inner plasma sheet and possible connection with SAPS and plasma sheet earthward flow bursts. *Journal of Geophysical Research: Space Physics*, *120*(6), 5009–5021. <https://doi.org/10.1002/2015JA021023>
- Lyons, L. R., Nishimura, Y., Xing, X., Runov, A., Angelopoulos, V., Donovan, E., & Kikuchi, T. (2012). Coupling of dipolarization front flow bursts to substorm expansion phase phenomena within the magnetosphere and ionosphere. *Journal of Geophysical Research*, *117*(A2), 2212. <https://doi.org/10.1029/2011JA017265>
- Lyons, L. R., Thorne, R. M., & Kennel, C. F. (1972). Pitch-angle diffusion of radiation belt electrons within the plasmasphere. *Journal of Geophysical Research*, *77*(19), 3455–3474. <https://doi.org/10.1029/JA077i019p03455>
- Ma, Q., Connor, H. K., Zhang, X. J., Li, W., Shen, X. C., Gillespie, D., et al. (2020). Global survey of plasma sheet electron precipitation due to whistler mode chorus waves in Earth's magnetosphere. *Geophysical Research Letters*, *47*(15), e88798. <https://doi.org/10.1029/2020GL088798>
- Ma, Q., Ni, B., Tao, X., & Thorne, R. M. (2012). Evolution of the plasma sheet electron pitch angle distribution by whistler-mode chorus waves in non-dipole magnetic fields. *Annales Geophysicae*, *30*(4), 751–760. <https://doi.org/10.5194/angeo-30-751-2012>
- Malaspina, D. M., Ukhorskiy, A., Chu, X., & Wygant, J. (2018). A census of plasma waves and structures associated with an injection front in the inner magnetosphere. *Journal of Geophysical Research*, *123*(4), 2566–2587. <https://doi.org/10.1002/2017JA025005>
- Malaspina, D. M., Wygant, J. R., Ergun, R. E., Reeves, G. D., Skoug, R. M., & Larsen, B. A. (2015). Electric field structures and waves at plasma boundaries in the inner magnetosphere. *Journal of Geophysical Research*, *120*(6), 4263. <https://doi.org/10.1002/2015JA021137>
- Matsumoto, H., Kojima, H., Miyatake, T., Omura, Y., Okada, M., Nagano, I., & Tsutsui, M. (1994). Electrostatic Solitary Waves (ESW) in the magnetotail: BEN wave forms observed by GEOTAIL. *Geophysical Research Letters*, *21*(25), 2915–2918. <https://doi.org/10.1029/94GL01284>
- McFadden, J. P., Carlson, C. W., Larson, D., Ludlam, M., Abiad, R., Elliott, B., et al. (2008). The THEMIS ESA plasma instrument and in-flight calibration. *Space Science Reviews*, *141*(1–4), 277–302. <https://doi.org/10.1007/s11214-008-9440-2>
- Mende, S. B., Harris, S. E., Frey, H. U., Angelopoulos, V., Russell, C. T., Donovan, E., et al. (2008). The THEMIS array of ground-based observatories for the study of auroral substorms. *Space Science Reviews*, *141*(1–4), 357–387. <https://doi.org/10.1007/s11214-008-9380-x>
- Meredith, N. P., Bortnik, J., Horne, R. B., Li, W., & Shen, X.-C. (2021). Statistical investigation of the frequency dependence of the chorus source mechanism of plasmaspheric hiss. *Geophysical Research Letters*, *48*(6), e2021GL092725. <https://doi.org/10.1029/2021GL092725>
- Mozer, F. S., Agapitov, O., Artemyev, A., Drake, J. F., Krasnoselskikh, V., Lejosne, S., & Vasko, I. (2015). Time domain structures: What and where they are, what they do, and how they are made. *Geophysical Research Letters*, *42*(10), 3627–3638. <https://doi.org/10.1002/2015GL063946>
- Mozer, F. S., Agapitov, O. V., Hull, A., Lejosne, S., & Vasko, I. Y. (2018). Pulsating auroras produced by interactions of electrons and time domain structures. *Journal of Geophysical Research*, *122*(8), 8604–8616. <https://doi.org/10.1002/2017JA024223>
- Muschietti, L., Ergun, R. E., Roth, I., & Carlson, C. W. (1999). Phase-space electron holes along magnetic field lines. *Geophysical Research Letters*, *26*(8), 1093–1096. <https://doi.org/10.1029/1999GL900207>
- Nakamura, R., Baumjohann, W., Schödel, R., Brittmacher, M., Sergeev, V. A., Kubyshkina, M., et al. (2001). Earthward flow bursts, auroral streamers, and small expansions. *Journal of Geophysical Research*, *106*(A6), 10791–10802. <https://doi.org/10.1029/2000JA000306>
- Newell, P. T., Sotirelis, T., & Wing, S. (2009). Diffuse, monoenergetic, and broadband aurora: The global precipitation budget. *Journal of Geophysical Research*, *114*(A9), A09207. <https://doi.org/10.1029/2009JA014326>
- Ni, B., Liang, J., Thorne, R. M., Angelopoulos, V., Horne, R. B., Kubyshkina, M., et al. (2012). Efficient diffuse auroral electron scattering by electrostatic electron cyclotron harmonic waves in the outer magnetosphere: A detailed case study. *Journal of Geophysical Research*, *117*(A1), 1218. <https://doi.org/10.1029/2011JA017095>
- Ni, B., Thorne, R. M., Shprits, Y. Y., & Bortnik, J. (2008). Resonant scattering of plasma sheet electrons by whistler-mode chorus: Contribution to diffuse auroral precipitation. *Geophysical Research Letters*, *35*(11), 11106. <https://doi.org/10.1029/2008GL034032>
- Nishimura, Y., Bortnik, J., Li, W., Angelopoulos, V., Donovan, E. F., & Spanswick, E. L. (2018). Comment on “pulsating auroras produced by interactions of electrons and time domain structures” by mozer et al. *Journal of Geophysical Research*, *123*(3), 2064–2070. <https://doi.org/10.1002/2017JA024844>
- Nishimura, Y., Lessard, M. R., Katoh, Y., Miyoshi, Y., Grono, E., Partamies, N., et al. (2020). Diffuse and pulsating aurora. *Space Science Reviews*, *216*(1), 4. <https://doi.org/10.1007/s11214-019-0629-3>
- Nishimura, Y., Lyons, L. R., Angelopoulos, V., Kikuchi, T., Zou, S., & Mende, S. B. (2011). Relations between multiple auroral streamers, pre-onset thin arc formation, and substorm auroral onset. *Journal of Geophysical Research*, *116*(A9), A09214. <https://doi.org/10.1029/2011JA016768>
- Paschmann, G., Haaland, S., & Treumann, R. (2002). Auroral plasma physics. *Space Science Reviews*, *103*, 1–19. <https://doi.org/10.1023/A:1023030716698>
- Scarf, F. L., Frank, L. A., Ackerson, K. L., & Lepping, R. P. (1974). Plasma wave turbulence at distant crossings of the plasma sheet boundaries and the neutral sheet. *Geophysical Research Letters*, *1*(5), 189–192. <https://doi.org/10.1029/GL001i005p00189>
- Sergeev, V. A., Angelopoulos, V., & Nakamura, R. (2012). Recent advances in understanding substorm dynamics. *Geophysical Research Letters*, *39*(5), 5101. <https://doi.org/10.1029/2012GL050859>
- Sergeev, V. A., Liou, K., Newell, P., Ohtani, S., Hairston, M., & Rich, F. (2004). Auroral streamers: Characteristics of associated precipitation, convection and field-aligned currents. *Annales Geophysicae*, *22*(2), 537–548. <https://doi.org/10.5194/angeo-22-537-2004>
- Shen, Y. (2024). Diffusion rates for GRL manuscript “Red line diffusion-like auroras driven by time domain structures associated with braking magnetotail flow bursts” [Dataset]. *Zenodo*. <https://doi.org/10.5281/zenodo.11044554>
- Shen, Y., Artemyev, A., Zhang, X.-J., Vasko, I. Y., Runov, A., Angelopoulos, V., & Knudsen, D. (2020). Potential evidence of low-energy electron scattering and ionospheric precipitation by time domain structures. *Geophysical Research Letters*, *47*(16), e89138. <https://doi.org/10.1029/2020GL089138>
- Shen, Y., Artemyev, A. V., Zhang, X.-J., Zou, Y., Angelopoulos, V., Vasko, I., et al. (2023). Contribution of kinetic Alfvén waves to energetic electron precipitation from the plasma sheet during a substorm. *Journal of Geophysical Research: Space Physics*, *128*(4), e2023JA031350. <https://doi.org/10.1029/2023JA031350>

- Shen, Y., Vasko, I. Y., Artemyev, A., Malaspina, D. M., Chu, X., Angelopoulos, V., & Zhang, X.-J. (2021). Realistic electron diffusion rates and lifetimes due to scattering by electron holes. *Journal of Geophysical Research: Space Physics*, *126*(9), e29380. <https://doi.org/10.1029/2021JA029380>
- Solomon, S. C., Hays, P. B., & Abreu, V. J. (1988). The auroral 6300 Å emission: Observations and modeling. *Journal of Geophysical Research*, *93*(A9), 9867–9882. <https://doi.org/10.1029/JA093iA09p09867>
- Tian, S., Colpitts, C. A., Wygant, J. R., Cattell, C. A., Ferradas, C. P., Igl, A. B., et al. (2021). Evidence of Alfvénic Poynting flux as the primary driver of auroral motion during a geomagnetic substorm. *Journal of Geophysical Research: Space Physics*, *126*(5), e29019. <https://doi.org/10.1029/2020JA029019>
- Tsyganenko, N. A. (1989). A magnetospheric magnetic field model with a warped tail current sheet. *Planetary and Space Science*, *37*(1), 5–20. [https://doi.org/10.1016/0032-0633\(89\)90066-4](https://doi.org/10.1016/0032-0633(89)90066-4)
- Vasko, I. Y., Agapitov, O. V., Mozer, F. S., Artemyev, A. V., Krasnoselskikh, V. V., & Bonnell, J. W. (2017). Diffusive scattering of electrons by electron holes around injection fronts. *Journal of Geophysical Research*, *122*(3), 3163–3182. <https://doi.org/10.1002/2016JA023337>
- Vasko, I. Y., Krasnoselskikh, V. V., Mozer, F. S., & Artemyev, A. V. (2018). Scattering by the broadband electrostatic turbulence in the space plasma. *Physics of Plasmas*, *25*(7), 072903. <https://doi.org/10.1063/1.5039687>
- Williams, J. D., Chen, L. J., Kurth, W. S., Gurnett, D. A., & Dougherty, M. K. (2006). Electrostatic solitary structures observed at Saturn. *Geophysical Research Letters*, *33*(6), L06103. <https://doi.org/10.1029/2005GL024532>
- Yadav, S., Lyons, L. R., Liu, J., Nishimura, Y., Tian, S., Zou, Y., & Donovan, E. F. (2022). Association of equatorward extending auroral streamers with ground magnetic perturbations and geosynchronous injections. *Journal of Geophysical Research: Space Physics*, *127*(11), e2022JA030919. <https://doi.org/10.1029/2022JA030919>
- Zhang, X.-J., Angelopoulos, V., Ni, B., & Thorne, R. M. (2015). Predominance of ECH wave contribution to diffuse aurora in Earth's outer magnetosphere. *Journal of Geophysical Research*, *120*(1), 295–309. <https://doi.org/10.1002/2014JA020455>